What Happens during the Picosecond Lifetime of $2A_1$ Cyclohexa-1,3-diene? A CAS-SCF Study of the Cyclohexadiene/Hexatriene Photochemical Interconversion

Paolo Celani,[†] Stefano Ottani,[‡] Massimo Olivucci,*[,†] Fernando Bernardi,[†] and Michael A. Robb*[,§]

Contribution from the Dipartimento di Chimica "G. Ciamician" dell' Università di Bologna, Via Selmi 2, 40126 Bologna, Italy, Centro di Studio per la Fisica delle Macromolecole del CNR, Via Selmi 2, 40126 Bologna, Italy, and Department of Chemistry, King's College, London, Strand, London WC2R 2LS, U.K.

Received March 31, 1994[⊗]

Abstract: The $2A_1$ potential energy surface of cyclohexadiene (CHD)/*cZc*-hexa-1,3,5-triene (*cZc*-HT) has been extensively investigated via *ab-initio* CAS-SCF and CAS-SCF/MP2 computations. In contrast with previous computational studies, the optimization of the $2A_1$ stationary points has been carried out with no structural constraints. Several important reaction pathways have been fully documented via computation of the intrinsic reaction coordinate (IRC). A complete mechanistic picture of the photochemical ring opening occurring on the $2A_1$ surface after CHD photoexcitation is presented. This picture is consistent with modern and older experimental data. The main $2A_1 \rightarrow 1A_1$ radiationless decay channel occurs in the region of a conical intersection located about 1 kcal mol^{-1} above the excited-state ring-opening product *cZc*-HT*. This finding is in contrast with the generally accepted notion that the $2A_1 \rightarrow 1A_1$ decay channel corresponds to a $2A_1$ avoided minimum. Indeed no avoided crossing minimum is found along the computed $2A_1$ ring-opening pathway.

1. Introduction

The use of picosecond time-resolved UV resonance Raman spectroscopy has recently allowed the first direct observation of the dynamics of the photochemical ring opening of cyclohexa-1,3-diene (CHD) and α-phellandrene in solution. Mathies and co-workers[1] have established that these molecules undergo a rapid (10 fs) radiationless decay from the $1B_2$ Franck–Condon region to the $2A_1$ covalent excited state. In both cases, Mathies' experiments indicate that the reaction trajectory continues to propagate for a significant amount of time on the $2A_1$ potential energy surface after the $1B_2 \rightarrow 2A_1$ decay. Radiationless decay then yields vibrationally hot ground-state hexa-1,3,5-triene (HT) with an appearance time of 6 ps after the initial CHD photoexcitation.[1a] Similarly, production of 3,7-dimethylocta-1,3,5-triene occurs with an appearance time of only 11 ps after α-phellandrene photoexcitation.[1a] Thus these experiments indicate that a lifetime of several picoseconds for the $2A_1$ state is a general feature of cyclohexadiene photochemistry. The analysis of the photoproduct spectral evolution[1a] shows that *cZc*-HT (i.e., *all-cis*-HT) is the first conformer to appear on the ground-state surface (see Scheme 1). The more stable *cZt*-HT conformer (i.e., *mono-s-cis*-HT) is then formed within 7 ps, presumably via thermal *cZc* to *cZt* conversion. These observations are consistent with earlier experimental work. Quantum yield measurements at low conversion[2a,b] show that *cZc*-hexatrienes are the only primary photoproducts of cyclohexadiene direct irradiation and

Scheme 1

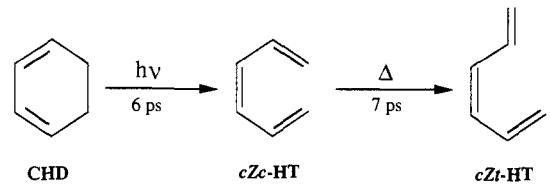

therefore are intermediates for the production of *E*-hexatrienes and long-term irradiation photoproducts.

Although direct production of *cZc*-HT from photoexcited CHD is now firmly established, CHD is displaced, during its short $1B_2$ lifetime, only a small distance along the ring-opening reaction coordinate.[1c] Thus the formation of *cZc*-HT must necessarily occur during the $2A_1$ lifetime. Accordingly, the chemically relevant part of the reaction pathway must be entered after $1B_2$ depopulation and therefore lies on the $2A_1$ potential energy surface. Our objective in this paper is the full documentation of the reaction paths accessed by the system during the picosecond lifetime of the $2A_1$ state. These results provide, for the first time, a complete mechanistic picture of the photochemical ring opening occurring after $1B_2 \rightarrow 2A_1$ decay.

2. Theoretical and Computational Methods

All the CAS-SCF results presented in this paper have been produced using the MC-SCF program distributed in Gaussian 92.[3a] However, in a few relevant cases, single-point CAS-SCF/MP2[3b,c] computations have been performed in order to probe the energetics of the surface at a level of theory beyond CAS-SCF. The rigorous location of excited-state minima, transition struc-

[†] Università di Bologna.
[‡] Centro di Studio per la Fisica delle Macromolecole del CNR.
[§] King's College, London.
[⊗] Abstract published in *Advance ACS Abstracts,* September 1, 1994.

(1) (a) Reid, P. J.; Doig, S. J.; Wickham, S. D.; Mathies, R. A. *J. Am. Chem. Soc.* **1993**, *115*, 4754. (b) Trulson, M. O.; Dollinger, G. D.; Mathies, R. A. *J. Chem. Phys.* **1989**, *90*, 4274. (c) Reid, P. J.; Doig, S. J.; Mathies, R. A. *Chem. Phys. Lett.* **1989**, *156*, 163.

(2) (a) Jacobs, H. J. C.; Havinga, E. Photochemistry of Vitamin D and Its Isomers and of Simple Trienes. In *Advances in Photochemistry*; Pitts, J. N., Jr., Hammond, G. S., Gollnick, K., Eds.; John Wiley & Sons: New York, 1979; Vol. 11, pp 305–373. (b) Dauben, W. G.; McInnis, E. L.; Mincho, D. M. Photochemical rearrangements in trienes. In *Rearrangements in ground and excited states*; Academic Press: London, 1980; Vol. 3, pp 91–129.

(3) (a) Frisch, M. J.; Trucks, G. W.; Head-Gordon, M.; Gill, P. M. W.; Wong, M. W.; Foresman, J. B.; Johnson, B. G.; Schlegel, H. B.; Robb, M. A.; Replogle, E. S.; Gomperts, R.; Andres, J. L.; Raghavachari, K.; Binkley, J. S.; Gonzalez, C.; Martin, R. L.; Fox, D. J.; Defrees, D. J.; Baker, J.; Stewart, J. J. P.; Pople, J. A. *Gaussian 92*, Revision B; Gaussian, Inc.: Pittsburgh, PA, 1992. (b) McDouall, J. J. W.; Peasley, K.; Robb, M. A. *Chem. Phys. Lett.* **1988**, *148*, 183. (c) Bernardi, F.; Bottoni, A.; Celani, P.; Olivucci, M.; Robb, M. A.; Venturini, A. *Chem. Phys. Lett.* **1992**, *192*, 229–235.

0002-7863/94/1516-10141$04.50/0

tures, calculations of intrinsic reaction coordinates (IRC),[4] and surface scannings have been carried out by using the methods available in Gaussian 92. In contrast, the rigorous location of the "funnels" corresponding to low-lying conical intersection points requires a nonstandard method which we will now briefly summarize. This nonstandard method has been implemented in a development version of Gaussian.

In a polyatomic system, the "noncrossing rule" (which holds for diatomics) loses its validity and two electronic states of the same spatial/spin symmetry may cross at a conical intersection.[5] Thus the photochemical reaction funnel (first discussed for organic systems by Zimmerman[6e] and Michl[6g]) corresponds to a conical intersection point and plays the central role in mechanistic photochemistry. At this point, decay to the lower state will occur within one vibrational period.[5c] Conical intersections have been extensively discussed in the literature,[6] and recent CAS-SCF investigations have indicated that the conical intersections can be a common feature in organic[7] and inorganic systems.[8]

The nature of the potential energy surfaces near a conical intersection point has been recently described by Ruedenberg et al.,[9] and it is convenient to use their terminology. In Scheme 2, we show a conical intersection of two potential energy surfaces as a "curve" spanning a $n-2$ dimensional subspace of the n nuclear coordinates called the *intersection space*.

While for any point belonging to the intersection space (i.e., any point of the curve in Scheme 2) the energies of the two states (i.e., E_0 and E_1) remain the same, the degeneracy is lifted when the geometry of the system is distorted along the two remaining linearly independent nuclear coordinates x_1 and x_2. Thus, when the energy of the two states is plotted in the *branching space* (i.e., against x_1 and x_2) as shown in Scheme 2, the corresponding potential energy surfaces looks like a double cone. The vectors x_1 and x_2 are directions defined by the nonadiabatic coupling (NADC) and gradient difference (GD) vectors, respectively. These vectors can be computed in the framework of CAS-SCF theory by using a set of state averaged orbitals as reported in ref 10. An optimized conical intersection structure corresponds to the lowest energy point (i.e., a minimum) in the n – 2 dimensional intersection space. The procedure we use for optimizing the structure of a conical intersection is based on a Newton–Lagrange technique and is fully documented in ref 10a.

Scheme 2

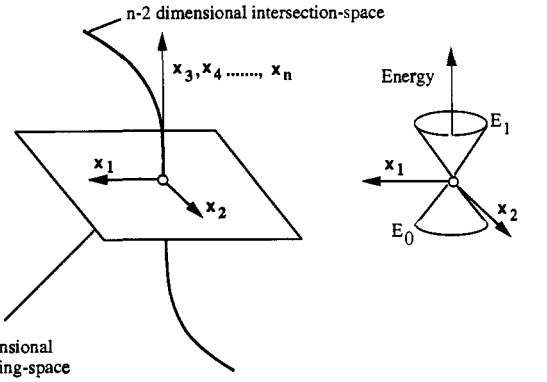

As discussed elsewhere,[7g] the vectors x_1 and x_2 have a dynamic significance which can be discussed qualitatively in the framework of simple semiclassical methods like the trajectory surface hopping (TSH) treatment.[11] The photoexcited system will move, during its excited-state lifetime, along classical trajectories that, in the limit of very low temperatures, can be represented by an IRC located on the excited-state sheet. When such a pathway terminates in the vicinity of a conical intersection point, the system undergoes a "surface hop", i.e. a radiationless decay from the upper to the lower state. In the limit of small momenta, the initial decay paths would lie in the branching space and therefore will follow the steepest descent lines on the lower potential energy sheet. In fact, at the minimum energy point on the conical intersection, the gradients of both the upper and lower states will be zero in all directions except x_1 or x_2. Thus the shape of the upper (E_1) and lower (E_0) potential energy sheets along the branching space contains information on the classical trajectories to and from the conical intersection.

To conclude this section, some comments on the reliability of the methods used are in order. There are three issues: the choice of active space in CAS-SCF computations, the basis set, and the role of dynamic correlation effects which are not included in CAS-SCF computations. The choice of active space in our computations is unambiguous and is comprised of the four electrons and orbitals which form the π-system of CHD plus the two CH_2–CH_2 σ and σ^* electrons and orbitals (or, equivalently, the six electrons and orbitals which form the π-system of HT). We have fully justified this choice of active space in other computations.[7h,i]

The most important consideration relates to limitations that arise from the basis set used and dynamic correlation. Since we have explored the excited-state surfaces and the conical intersection region in considerable detail, we have restricted ourselves to the modest 4-31G and DZ+d (double-ζ Dunning-Huzinaga + d-type polarization functions (heavy atoms only)) basis sets. These are adequate to determine the surface topology and optimized

(4) (a) Truhlar, D. G.; Steckler, R. *Chem. Rev.* **1987**, *87*, 217. Truhlar, D. G.; Gordon, M. S. *Science* **1990**, *249*, 491. (c) Gonzales, C.; Schlegel, H. B. *J. Phys. Chem.* **1990**, *94*, 5523.

(5) (a) Koppel, H.; Domcke, W.; Cederbaum, L. S. *Adv. Chem. Phys.* **1984**, *57*, 59. (b) Whetten, R. L.; Ezra, G. S.; Grant, E. R. *Rev. Phys. Chem.* **1985**, *36*, 277. (c) See, for example: Manthe, U.; Koppel, H. *J. Chem. Phys.* **1990**, *93*, 1658.

(6) (a) Von Neunann, J.; Wigner, E. *Phys. Z.* **1929**, *30*, 467. (b) Teller, E. *J. Phys. Chem.* **1937**, *41*, 109. (c) Herzberg, G.; Longuet-Higgins, H. C. *Trans. Faraday Soc.* **1963**, *35*, 77. (d) Herzberg, G. *The Electronic Spectra of Polyatomic Molecules*; Van Nostrand, Princeton, NJ, 1966; p 442. (e) Zimmerman, H. E. *J. Am. Chem. Soc.* **1966**, *88*, 1566. (f) Tully, J. C.; Preston, R. K.; *J. Chem. Phys.* **1971**, *55*, 562. (g) Michl, J. *J. Mol. Photochem.* **1972**, 243. (h) Zimmerman, H. E. *Acc. Chem. Res.* **1972**, *7*, 393. (i) Gerhartz, W. Poshusta, R. D.; Michl, J. *J. Am. Chem. Soc.* **1977**, *99*, 4263. (j) Davidson, R. E.; Borden, W. T.; Smith, J.; *J. Am. Chem. Soc.* **1978**, *100*, 3299–3302. (k) Mead, C. A.; Truhlar, D. G. *J. Chem. Phys.* **1979**, *70*, 2284. (l) Mead, C. A. *Chem. Phys.* **1980**, *49*, 23. (m) Keating, S. P.; Mead, C. A. *J. Chem. Phys.* **1985**, *82*, 5102. (n) Dehareng, D.; Chapuisat, X.; Lorquet, J. C.; Galloy, C.; Raseev, G. *J. Chem. Phys.* **1983**, *78*, 1246–1264. (o) Keating, S. P.; Mead, C. A. *J. Chem. Phys.* **1987**, *86*, 2152. (p) Bonacic-Koutecky, V.; Koutecky, J.; Michl, J. *Agnew. Chem., Int. Ed. Engl.* **1987**, *26*, 170–189. (q) Mead, C. A. The Born-Oppenheimer approximation in molecular quantum mechenics. In *Mathematical frontiers in computational chemical physics*; Truhlar, D. G., Ed.; Springer: New York, 1987; Chapter 1, pp 1–17. (r) Blais, N. C.; Truhlar, D. G.; Mead, C. A. *J. Chem. Phys.* **1988**, *89*, 6204–6208. (s) Michl, J.; Bonacic-Koutecky, V. *Electronic Aspects of Organic Photochemistry*; Wiley: New York, 1990.

(7) (a) Bernardi, F.; De, S.; Olivucci, M.; Robb, M. A. *J. Am. Chem. Soc.* **1990**, *112*, 1737–1744. (b) Bernardi, F.; Olivucci, M.; Robb, M. A. *Acc. Chem. Res.* **1990**, *23*, 405–412. (c) Bernardi, F.; Olivucci, M.; Ragazos, I. N.; Robb, M. A. *J. Am. Chem. Soc.* **1992**, *114*, 2752–2754. (d) Bernardi, F.; Olivucci, M.; Robb, M. A. *J. Am. Chem. Soc.* **1992**, *114*, 5805–5812. (e) Bernardi, F.; Olivucci, M.; Ragazos, I. N.; Robb, M. A. *J. Am. Chem. Soc.* **1992**, *114*, 8211–8220. (f) Palmer, I.; Bernardi, F.; Olivucci, M.; Robb, M. A. *J. Org. Chem.* **1992**, *57*, 5081–5087. (g) Olivucci, M.; Ragazos, I. N.; Bernardi, F.; Robb, M. A. *J. Am. Chem. Soc.* **1992**, *114*, 8211–8220. (h) Palmer, I. J.; Ragazos, I. N.; Bernardi, F.; Olivucci, M.; Robb, M. A. *J. Am. Chem. Soc.* **1993**, *115*, 673. (i) Olivucci, M.; Bernardi, F.; Ottani, S.; Robb, M. A. *J. Am. Chem. Soc.* **1994**, in press. (j) Woywod, C.; Domcke, W.; Sobolewski, A. L.; Werner, H.-J. *J. Chem. Phys.* **1994**, *100*, 1400.

(8) (a) Atchity, G. J.; Xantheas, S. S.; Elbert, S. T.; Ruedenberg, K. *J. Chem. Phys.* **1991**, *94*, 8054–8069. (b) Atchity, G. J.; Xantheas, S. S.; Elbert, S. T.; Ruedenberg, K. *Theor. Chim. Acta* **1991**, *78*, 365. (c) Muller, H.; Koppel, H.; Cederbaum, L. S.; Schmelz, T.; Chambaud, G.; Rosmus, P. *Chem. Phys. Lett.* **1992**, *197*, 599–606. (d) Manaa, M. R.; Yarkony, D. R. *J. Chem. Phys.* **1990**, *93*, 4473. (e) Manaa, M. R.; Yarkony, D. R. *J. Chem. Phys.* **1992**, *97*, 715–717.

(9) Atchity, G. J.; Xantheas, S. S.; Ruedenberg, K. *J. Chem. Phys.* **1991**, *95*, 1862–1876.

(10) (a) Ragazos, I. N.; Robb, M. A.; Bernardi, F.; Olivucci, M. *Chem. Phys. Lett.* **1992**, *197*, 217–223. (b) Yarkony, R. D. *J. Phys. Chem.* **1993**, *97*, 4407.

(11) (a) Tully, J. C.; Preston, R. K. *J. Chem. Phys.* **1971**, *55*, 562. (b) Dehareng, D.; Chapuisat, X.; Lorquet, J. C.; Galloy, C.; Raseev, G. *J. Chem. Phys.* **1983**, *78*, 1246–1264. (c) Blais, N. C.; Truhlar, D. G.; Mead, C. A. *J. Chem. Phys.* **1988**, *89*, 6204–6208.

geometries of the covalent states. Roos *et al.*[12a-d] have run accurate benchmark computations on the excited states of benzene, *s-trans*-butadiene, *all-trans*-hexatriene, and *all-trans*-octatetraene. They show that, while the description of the ionic (B_u) and Rydberg states is sensitive to basis sets, the number of active orbitals, and electron correlation, the covalent states are well described by small active spaces and without electron correlation correction. The quality of the DZ+d basis set used in our computations has been tested against the ANO basis set used by Roos for the computation of the excitation energies of the *s-trans*-butadiene and *all-trans*-hexatriene $2A_g$ states. Using ground-state CAS-SCF/DZ+d-optimized geometries for these two systems, we have been able to reproduce the published CAS-SCF/ANO data[12d] within the reported computational error. Our calculations therefore offer a reliable description of the lowest energy singlet covalent states which are of central importance[13] in the photochemical and photophysical processes. In order to confirm that the existence of the conical intersection points is not sensitive to dynamic correlation, we have performed a few computations in the conical intersection region with the CAS-SCF/MP2 method[4b] using the DZ+d basis set. As we will see below, these tests show that inclusion of dynamic correlation does not significantly affect the energy degeneracy at the optimized conical intersection.

3. Characterization of the $2A_1$ Potential Energy Surface

In this section we report the results of an extensive CAS-SCF and CAS-SCF/MP2 computational study of the $2A_1$ energy surface of CHD. These results provide a very complete mechanistic picture of the photochemical ring opening occurring after $1B_2 \rightarrow 2A_1$ decay. While a one-dimensional cross section[14a] of the potential surfaces has been reported previously,[14b] these results are misleading because the cross section is obtained by interpolating between ground-state geometries. We begin with an overview of the main results before a more detailed discussion begins.

The main features of our computations on the photochemical ring opening of CHD are summarized in Figure 1. We have used a two-dimensional cross section of the $2A_1$ and $1A_1$ potential energy surface of CHD (see caption for computational detals). Close to the Franck–Condon region, we have characterized a shallow cyclic CHD* excited-state minimum on the $2A_1$ surface. It is at this point that the excited-state reaction path will begin (after decay from the $1B_2$ state). The reaction path then leads, via an almost barrierless ring-opening process, to formation of the open-chain *cZc*-HT* intermediate. The depopulation of the $2A_1$ state and subsequent formation of ground-state *cZc*-HT then occurs via a large-amplitude vibration from the *cZc*-HT* minimum. This vibration, in the lowest frequency *cZc*-HT* normal mode, leads to efficient radiationless decay through a $2A_1/1A_1$ conical intersection point (CI_{CHD}) located slightly above ($\sim$1 kcal mol^{-1}) the minimum. Since CI_{CHD} is located at the top of two different ground-state valleys, the $2A_1$ reaction pathway bifurcates on the ground-state surface.

The electronic structure and energy of the system in the region surrounding the CI_{CHD} conical intersection provide a simple explanation for various experimental features. The observed $\sim$0.4 CHD ring-opening quantum yield[2] is consistent with ground-state bifurcation which leads to competitive formation of *cZc*-HT and back-formation of the original reactant (see arrows on the lower sheet of Figure 1). The computed *cZc*-HT* $\rightarrow$ CI_{CHD} energy barrier is consistent with the picosecond appearance time measured for *cZc*-HT. In general, one can see that photoexcitation of both CHD and *cZc*-HT must generate the same *cZc*-HT* intermediate. Thus *cZc*-HT* may be regarded as the "hub" of CHD/HT photochemical interconversion. We now proceed to document the reaction mechanism outlined above in some detail. In the next section we will compare our results with the experiment.

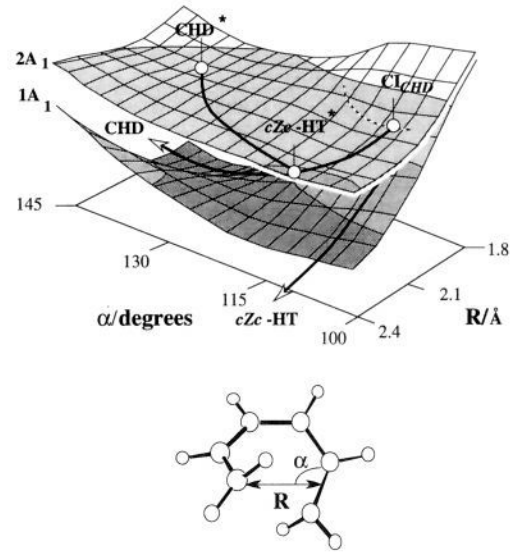

Figure 1. CAS-SCF/4-31G two-dimensional cross section of the $2A_1$ and $1A_1$ potential energy surfaces of CHD. The surfaces have been computed via two-dimensional scanning (55 grid nodes) along the geometrical parameters R and α. The values of the remaining 34 CHD geometrical parameters have been optimized at each surface grid node with respect to the $2A_1$ energy. The full lines represent the reaction paths connecting different regions of the $2A_1$ surface (see text for labels). The dashed line on the $2A_1$ surface intercepts the region where the two surfaces are degenerate.

The $2A_1$ surface cross section in Figure 1 shows two basic mechanistic features of the CHD photochemical ring-opening reaction. These are (i) a CHD* $\rightarrow$ *cZc*-HT* reaction pathway, which leads to production of excited-state HT, and (ii) a *cZc*-HT* decay pathway, which leads to formation of the final photoproduct. These pathways will be discussed in detail in subsections i and ii below. While pathway ii is found to be the most favorable decay pathway from *cZc*-HT*, a series of different decay/reaction paths leading to Z/E and c/t isomerization and twisting of a terminal CH_2 group have also been located on the same excited-state surface. These alternative pathways are much higher in energy and will be described in subsection iii. The absolute and relative energies of all the stationary points and conical intersections are documented in Table 1.

(i) Relaxation on the $2A_1$ Surface: CHD* $\rightarrow$ *cZc*-HT* Reaction Pathway. We begin with a discussion of the relaxation on the $2A_1$ surface corresponding to the CHD* $\rightarrow$ *cZc*-HT* reaction pathway shown in Figure 1. This pathway has been documented by characterizing (a) the local minima corresponding to CHD* (shown in Figure 2 together with the equilibrium structure of ground-state CHD) and *cZc*-HT* and (b) the CHD* $\rightarrow$ *cZc*-HT* transition state (TS_{CHD}) and reaction coordinate (obtained from an IRC computation) shown in Figure 3.

As the system moves along the ring-opening route, the C_2-symmetry CHD* structure undergoes an almost barrierless excited-state rearrangement to *cZc*-HT*. From inspection of Figure 3, it is evident from the geometry of TS_{CHD} and structure I that, in contrast to what expected for a "classic" conrotatory path, the reaction coordinate does not conserve C_2 symmetry.

(12) (a) Serrano-Andrés, L.; Merchan, M.; Nebot-Gil, I.; Lindh, R.; Roos, B. O. *J. Chem. Phys.* **1993**, *98*, 3151–3162. (b) Matos, J. M. O.; Roos, B. O.; Malmqvist, P.-Å. *Chem. Phys.* **1987**, *86*, 1458–1466. (c) Roos, B. O.; Andersson, K.; Fülscher, M. P. *Chem. Phys. Lett.* **1992**, *192*, 5–13. (d) Serrano-Andres, L.; Merchan, M.; Nebot-Gil, I.; Lindh, R.; Roos, B. O. *J. Chem. Phys.* **1993**, *98*, 3151–3162.

(13) (a) Petek, H.; Bell, A. J.; Christensen, R. L.; Yoshihara, K.; *J. Chem. Phys.* **1992**, *96*, 2412–2415. (b) Ci, X.; Myers, A. B. *J. Chem. Phys.* **1992**, *96*, 6433–6441. (c) Buma, W. J.; Kohler, B. E.; Song, K. *Chem. Phys.* **1991**, *94*, 6367–6375.

(14) (a) Share, P. E.; Kompa, K. L.; Peyerimhoff, S. D.; Van Hemert, M. C. *Chem. Phys.* **1988**, *120*, 411. (b) For previous (semiempirical) computations on the *cZc*-HT $\rightarrow$ CHD conversion, see also: Pichko, V. A.; Simkin, B. Y., Minkin, V. I. *J. Org. Chem.* **1992**, *57*, 7087.

Table 1. Absolute (E) and Relative (ΔE) CAS-SCF and CAS-SCF/MP2 (Values in Brackets) Energies for the Stationary Points and Conical Intersections of S_1 ($2A_1$) of Cyclohexadiene (CHD) and *cZc*-Hexatriene (*cZc*-HT)

structure	root	E/4-31G (au)	E/DZ+d (au)	ΔE/4-31G (kcal mol^{-1})	ΔE/DZ+d (kcal mol^{-1})
cZc-HT	S_0	−231.553 33	−231.904 14	−87.8	−85.7
CHD	S_0	−231.573 92	231.935 51	−100.8	−103.5
cZc-HT*	S_1	−231.413 35	−231.767 61	0.0	0.0
			(−232.484 88)		(0.0)
cZc-HT*	S_0	−231.480 64	−231.822 06	−42.2	−34.2
C_2-HT*	S_1		−231.766 42		0.7
CHD*	S_1	−231.384 97	−231.746 77	17.8	13.1
TS_{CHD}	S_1	−231.383 79	−231.747 13	18.5	13.1
$TS_{Cl_{c/t}}$	S_1	−231.384 78	−231.742 13	17.9	16.0
			(−232.447 18)		(23.7)
$TS_{Cl_{Z/E}}$	S_1	−231.374 06	−231.731 52	24.7	22.6
			(−232.437 76)		(29.5)
TS_{CH_2}	S_1	−231.382 37	−231.736 28	19.4	19.7
$TS_{c/t}$	S_1	−231.361 90	−231.716 39	32.3	32.1
$TS_{Z/E}$	S_1	−231.376 61	−231.730 53	23.1	23.3
FP_{CHD}[b]	S_1	−231.403 88	−231.757 35	5.9	6.4
FP_{IRD}[b]	S_1	−231.406 86	−231.762 57	4.1	3.2
			(−232.483 81)		(0.7)
CI_{CHD}	S_1[c]	−231.386 91	−231.739 24[d]		
			(−232.459 08)[d]		
CI_{CHD}	S_0[c]	−231.387 14	−231.744 30[d]		
			(−232.467 70)[d]		
$CI_{c/t}$	S_1[c]	−231.380 83	−231.735 44[d]		
$CI_{c/t}$	S_0[c]	−231.382 89	−231.738 87[d]		
$CI_{Z/E}$	S_1[c]	−231.369 63	−231.724 06[d]		
$CI_{Z/E}$	S_0[c]	−231.369 99	−231.721 58[d]		

[a] A few relevant S_0 ($1A_1$) energy values have also been included in the table. [b] This structure does not correspond to a stationary point. See text. [c] Indicates a state-averaged CAS-SCF calculation. See ref 10. [d] Energy value computed at the CAS-SCF/4-31G-optimized structure.

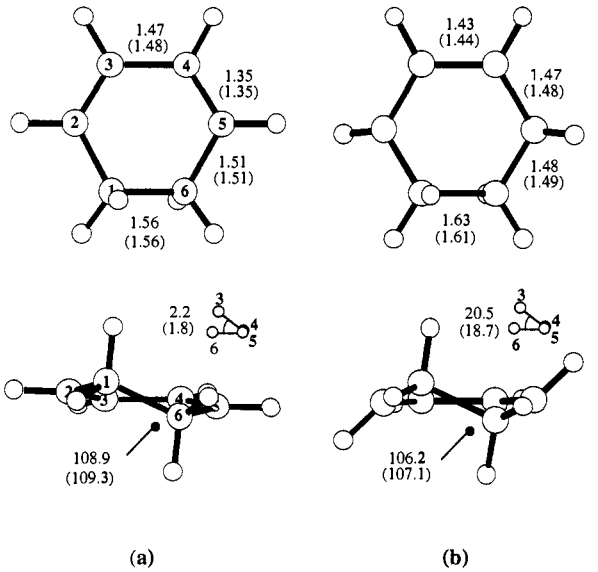

Figure 2. Optimized CAS-SCF ground-state CHD (a) and excited-state CHD* (b) equilibrium structures. The main structural parameters are reported (bond lengths in Å and bond angles in deg) for both the 4-31G and DZ+d (in brackets) results.

Consequently, the molecular structure of the final excited-state product *cZc*-HT* is slightly asymmetric. At the *cZc*-HT* minimum, the lowest frequency (135 cm^{-1}) vibration is associated with a nontotally symmetric molecular displacement. Thus *cZc*-HT* is located at the bottom of a very flat double well with a transition state with C_2 symmetry (C_2-HT* in Table 1). The barrier to the interconversion of these minima is only 0.7 kcal mol^{-1}.

The IRC energy profile (plotted as a function of the C_1–C_6 bond length in Figure 4) demonstrates two important features of the CHD* → *cZc*-HT* pathway. Firstly, the excited-state/

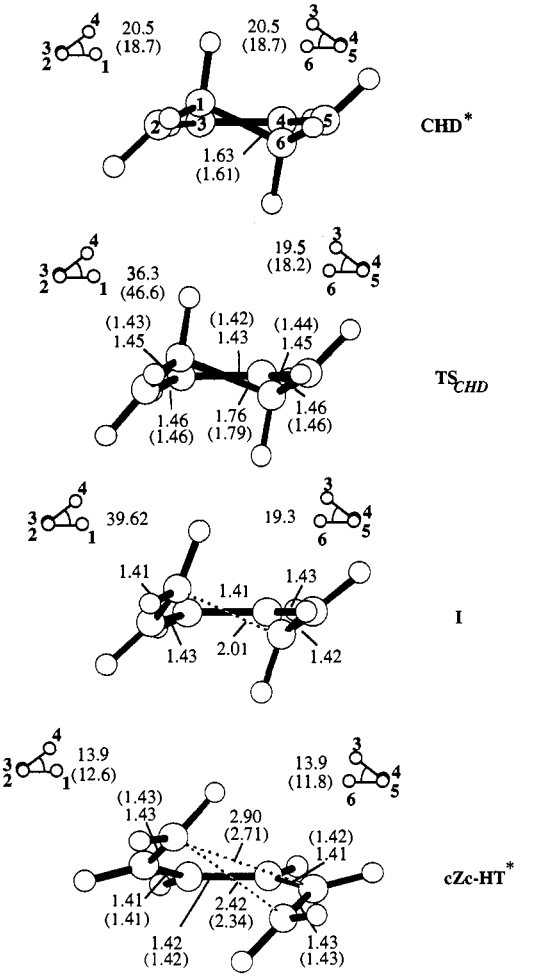

Figure 3. Evolution of the CHD* equilibrium structure along the CHD* → *cZc*-HT* IRC computed at the CAS-SCF 4-31G level. TS_{CHD} indicates the transition structure, and I indicates a nonstationary point located along the IRC (see Figure 4). The main structural parameters are reported (bond lengths in Å and bond angles in deg) for both the 4-31G and DZ+d (in brackets) results. The DZ+d results are given for stationary points only.

ground-state energy gap is always greater than 30 kcal mol^{-1}. Secondly, along the ground-state curve, there are two local minima located at the same geometries as the excited-state CHD* and *cZc*-HT* structures. *Further, there is no excited-state minimum in the region of the maximum of the ground-state energy profile.* Thus, efficient internal conversion cannot take place along this IRC and there is no effective $2A_1/1A_1$ decay route along this path. This observation is in striking contrast to the potential energy cross section investigated by Share et al.[14] using a reaction coordinate interpolated between the ground-state equilibrium geometries of CHD and *cZc*-HT. Along such a coordinate, Share et al. find a deep excited-state minimum at the same geometry as the ground-state maximum and therefore suggest that $2A_1 \rightarrow 1A_1$ internal conversion takes place at this point. The energy profile shown in Figure 4 does not show such a feature and thus demonstrates the importance of IRC computations for studying excited-state reaction pathways.

(ii) *cZc*-HT* Decay via the CI_{CHD} Conical Intersection. Vibrational motion of *cZc*-HT* along its lowest frequency normal mode (shown in Figure 5a) leads the system toward the conical intersection CI_{CHD} shown in Figure 5b (where the $2A_1$ and $1A_1$ potential energy surfaces are degenerate and fully efficient $2A_1 \rightarrow 1A_1$ decay takes place). The change in the *cZc*-HT* geometry associated with this motion (Figure 5a) is dominated by a decrease in C_1–C_5 distance accompanied by a smaller decrease in C_1–C_6 distance coupled with relaxation of the C_2–C_3–C_4 moiety. We shall now discuss the details of the *cZc*-HT* decay path via the

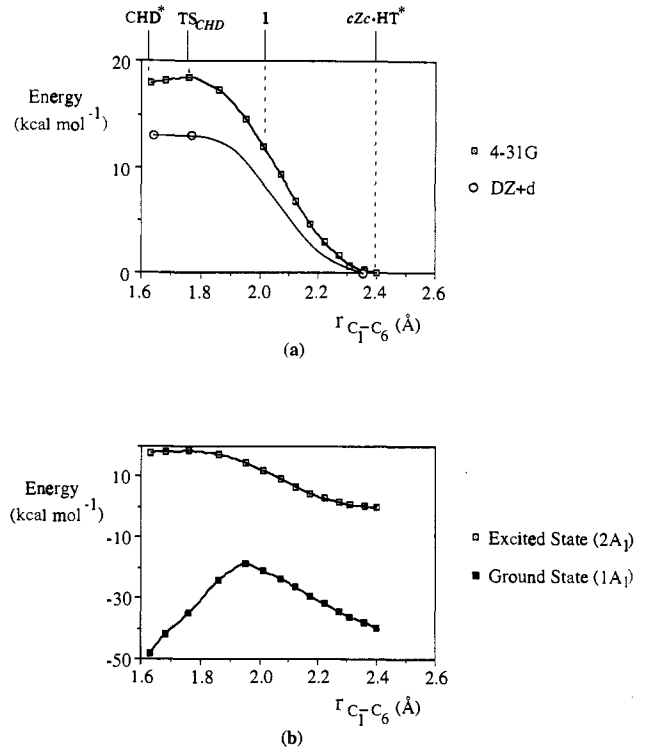

Figure 4. (top) Excited-state energy profiles along the CHD* → *cZc*-HT* IRC computed at the CAS-SCF/4-31G level and plotted against the C_1–C_6 distance ($r_{C_1-C_6}$). The position and energy of the CAS-SCF/DZ+d stationary point structures have also been reported in the figure. (bottom) Comparison of the excited- and ground-state energy profiles along the same IRC computed at the CAS-SCF/4-31G level.

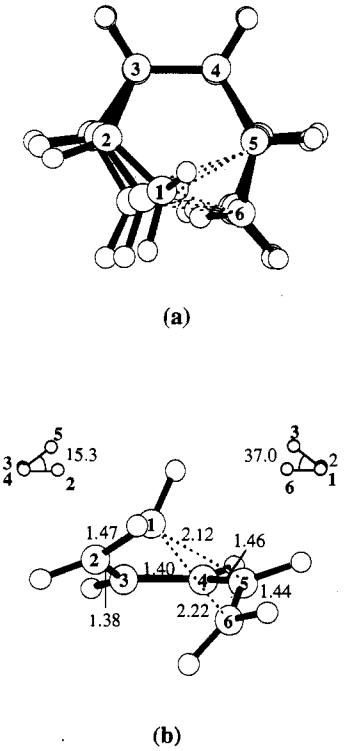

Figure 5. (a) Schematic representation of the lowest (135 cm^{-1}) frequency normal mode (computed at the CAS-SCF/4-31G level) of the *cZc*-HT*. Bottom to top structures illustrate the geometrical deformation of *cZc*-HT* associated to this mode. (b) Optimized CAS-SCF/4-31G CI_{CHD} conical intersection structure. The values of the more important bond lengths and bond angles are given in Å and deg.

CI_{CHD} conical intersection. This path has been documented by (a) characterization of the CI_{CHD} conical intersection and (b) computation of a *cZc*-HT* → CI_{CHD} IRC starting from a point on the $2A_1$ potential energy surface located in the immediate vicinity of CI_{CHD} (point FP_{CHD} in Table 1).

The molecular structure corresponding to CI_{CHD} has been optimized at the CAS-SCF 4-31G level using the method briefly outlined in section 2, and its structural parameters are reported in Figure 5b. The stability of the degeneracy between the first and second roots at CI_{CHD} has been tested by improving the basis set (i.e., using the DZ+d basis set) and by performing CAS-SCF/MP2 computations (see section 2) with the DZ+d basis set. The results in Table 1 demonstrate that neither the improvement of the basis set nor the evaluation of dynamic correlation energy via CAS-SCF/MP2 removes the degeneracy (small S_1/S_0 gaps in Table 1, around 3 kcal mol^{-1}, arise because the energies are evaluated via single-point computations on CI_{CHD} optimized at the CAS-SCF 4-31G level).

We now comment on the rather unusual molecular structure of CI_{CHD}. The C_1–C_5 and C_1–C_6 distances are almost equal so that C_1, C_5, and C_6 form a quasi-isosceles triangle. Further, the C_2–C_3–C_4 fragment has a geometrical structure very close to that of a ground-state allyl radical. In fact, both the geometry and wave function of CI_{CHD} suggest that this structure corresponds to a quasi-tetraradical with four weakly interacting electrons. Three of these electrons are localized on carbons C_1, C_2, and C_3, respectively, while the fourth electron is delocalized on the C_2–C_3–C_4 allyl fragment. CI_{CHD} belongs to a class of conical intersections which have been already described in the past (e.g., the addition of a CH_3 radical to ethylene[15] where a C_{2v} conical intersection exists between the ground state and the first doublet excited state with a structure which closely resembles the triangular moiety in CI_{CHD}). Further, one can easily recognize that this type of conical intersection is related, both electronically and geometrically, to the well-known H_3 conical intersection[16] which has a rigorously equilateral triangle structure. It is possible to rationalize this rather unusual structure using valence bond arguments.[15]

The IRC energy profiles, along the coordinate connecting *cZc*-HT* to CI_{CHD} starting from a point of the $2A_1$ potential energy surface located in the immediate vicinity of CI_{CHD} (point FP_{CHD}), are reported in Figure 6a as a function of the distance C_1–C_5. The evolution of the molecular structure along this IRC is virtually identical with the low-frequency large-amplitude vibration of *cZc*-HT* shown in Figure 5a. The gap between the $1A_1$ and $2A_1$ energy profiles decreases rapidly up to a point where the two curves cross along the coordinate connecting *cZc*-HT* to CI_{CHD} (i.e., decreasing the C_1–C_5 distance).

The slope of this energy profile between *cZc*-HT* and CI_{CHD} and thus the value of the barrier to the conical intersection are sensitive to the level of theory used in the computation. An accurate estimate of the energy barrier has been further obtained via CAS-SCF/MP2 single-point computations with the DZ+d basis set. The CAS-SCF/MP2 energy has been computed at both the optimized *cZc*-HT* structure and the first IRC point (FP_{IRC} in Table 1 and Figure 6). The results indicate that MP2 correction of the CAS-SCF DZ+d energy yields a flatter *cZc*-HT* → CI_{CHD} energy profile and, in turn, a lower energy barrier to CI_{CHD}. In contrast, the corresponding ground-state ($1A_1$) energy profile is only marginally affected by the MP2 correction. The *cZc*-HT* → CI_{CHD} energy profile corresponds to a nearly harmonic potential. Thus a quadratic fit (Figure 6b) of the CAS-SCF DZ+d energies as a function of the distance along the IRC successfully interpolates all points. Assuming that the shape of the potential well remains quadratic after MP2 correction, a more accurate *cZc*-HT → CI_{CHD} barrier can be derived using the computed CAS-SCF/MP2 energies. In Figure 6b, we see that extrapolation of the $2A_1$ and $1A_1$ CAS-SCF/MP2 quadratic

(15) Bernardi, F.; Olivucci, M.; Robb, M. A. *Is. J. Chem.* **1993**, *22*, 265.
(16) See: Wu, Y. M.; Kupperman, A. *Chem. Phys. Lett.* **1993**, *201*, 178 and references cited therein.

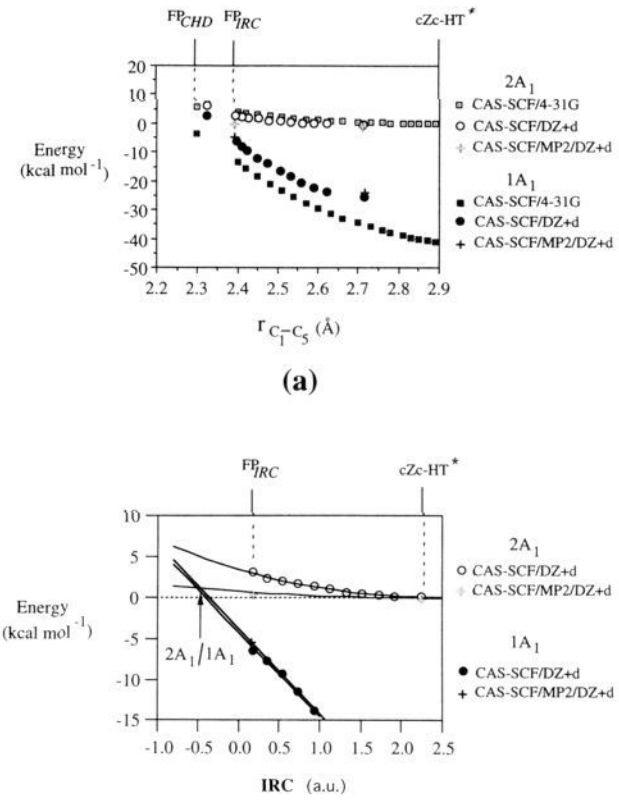

Figure 6. (a) Excited ($2A_1$)- and ground ($1A_1$)-state energy profiles along the *cZc*-HT* → CI_{CHD} IRC computed at different levels of theory and plotted against the C_1–C_5 distance ($r_{C_1-C_5}$). IRC computations were started from the nonstationary point FP_{CHD}. (b) Quadratic fittings of the CAS-SCF/DZ+d and CAS-SCF/MP2/DZ+d *cZc*-HT* → CI_{CHD} IRC's. Extrapolation of the CAS-SCF/MP2/DZ+d results yields the $2A_1/1A_1$ crossing point (i.e., CI_{CHD}) energy at this level of theory.

Scheme 3

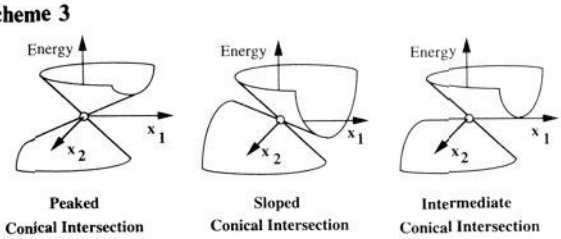

curves gives a $2A_1/1A_1$ crossing point lying about 1.0 kcal mol^{-1} above the *cZc*-HT* minimum.

In order to understand, qualitatively, the dynamics of the decay via the conical intersection, we have characterized the local topology of this region of the potential surface in more detail. This characterization is accomplished by a discussion of the "orientation" of the two-dimensional branching space (x_1, x_2) shown in Scheme 2 with respect to the IRC vector (which coincides with the low-frequency large-amplitude vibration of *cZc*-HT* shown in Figure 5a). In fact, as mentioned above, the shape and orientation of the upper and lower potential energy surface along the branching space provide information on the classical trajectories to and from the conical intersection.

For the discussion of the local topology of the conical intersection, it is convenient to use the topological classification used by Ruedenberg et al.[9] There are two main conical intersection shapes, "peaked" and "sloped", which are shown in Scheme 3. An "intermediate" shape is also possible.

Comparison of Figure 6 and Scheme 3 indicates that the local topology of the $2A_1$ and $1A_1$ energy surfaces at CI_{CHD} corresponds

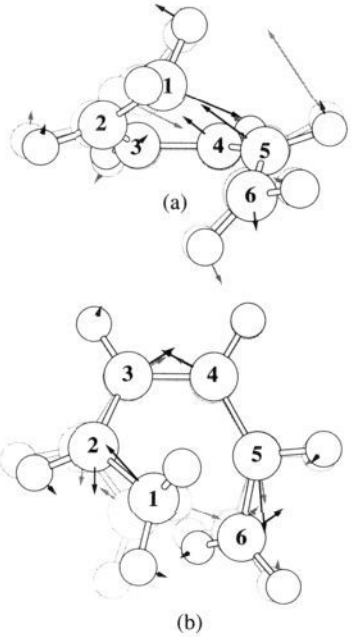

Figure 7. (a) Optimized CAS-SCF/4-31G CI_{CHD} conical intersection structure (same as in Figure 5b). Full arrows indicate the direction of the main atomic displacements corresponding to the computed x_1 vector. Light arrows indicate the direction of the main atomic displacements corresponding to the lowest frequency normal mode computed at FP_{IRC}. (b) Same as part a but the full arrows indicate the direction of the main atomic displacements corresponding to the computed x_2 vector and the light arrows indicate the direction of the main atomic displacements corresponding to the asymmetric stretching of the carbon framework computed at FP_{IRC}.

to that of a "sloped" conical intersection where some coordinate on the branching space correlates with the *cZc*-HT* → CI_{CHD} IRC. We now discuss this point in a little more detail with reference to the CAS-SCF/4-31G x_1 and x_2 vectors shown in Figure 7 computed at the CI_{CHD}-optimized structure. (The computation of the vectors x_1 and x_2 has been briefly discussed in section 2.)

The orientation of the branching space, relative to the IRC can be documented via the projections of the FP_{IRC} normal modes (computed via a numerical frequency computation) onto x_1 and x_2. (FP_{IRC} is the (optimized) IRC point closest to CI_{CHD}.) There are only two modes with a large projection onto the branching space. The first mode has projections 0.6 and –0.1 and corresponds to the IRC vector itself. The second mode has projections 0.2 and 0.8 and corresponds to the asymmetric stretching of the FP_{IRC} carbon framework. Thus, the projected IRC is almost parallel to x_1 and the projection of the asymmetric-stretching mode is almost parallel to the x_2 vector. This observation is apparent from Figure 7, where we compare the geometry deformations corresponding to the x_1 and x_2 vectors with the corresponding FP_{IRC} modes (faint structure and arrows). In Figure 8, we show the upper ($2A_1$) and lower ($1A_1$) potential energy sheets in the branching space as a function of the coordinates defined by x_1 and x_2 (see caption for computational details). One can observe that the degeneracy associated with the conical intersection is lifted when the geometry is distorted in the plane x_1x_2. It is also evident from this figure that CI_{CHD} corresponds to a slightly "sloped" conical intersection of the type shown in Scheme 3. The IRC from *cZc*-HT* enters the conical intersection along x_1. The coordinate x_2 corresponds to a higher frequency mode which correlates with the 2349 cm^{-1} (CAS-SCF/4-31G) asymmetric stretching at the *cZc*-HT* minimum.

In conclusion, our computations demonstrate that a low-lying, easily accessible, sloped conical intersection exists on the excited-state potential energy surface of CHD. The shape of this conical

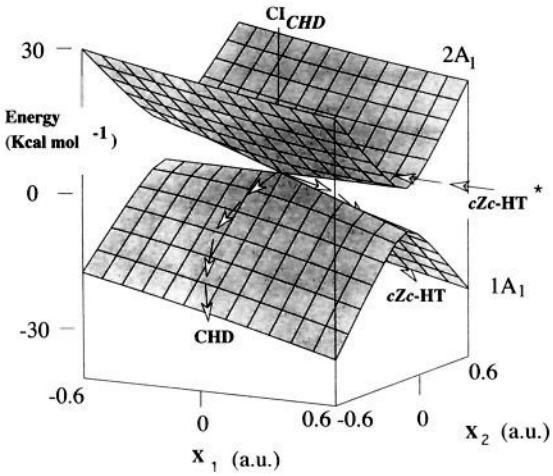

Figure 8. Analytical representation of the $2A_1$ and $1A_1$ energy surfaces plotted along the branching space (x_1, x_2). Coordinate x_1 correlates with the *cZc*-HT* → CI_{CHD} IRC. Coordinate x_2 correlates with the asymmetric stretching of the carbon framework computed at FP_{IRC}. The surfaces are constructed according to eq 3.3 in ref 9 using the $2A_1$ and $1A_1$ gradients computed at CI_{CHD} and FP_{IRC} at the CAS-SCF/4-31G level.

intersection and the nature of the x_1 and x_2 coordinates spanning the branching space provide the basis for explaining the less-than-one HT quantum yield observed during photolysis of CHD. We shall discuss this subsequently.

(iii) Alternative *cZc*-HT* Decay Pathways Leading to *Z*/*E* and *c*/*t* Isomerization and CH_2 Twisting. The excited-state *cZc*-HT* intermediate might evolve along alternative pathways involving *Z*/*E* or *c*/*t* isomerization of the HT framework or twisting of one of the terminal CH_2 groups. Such pathways lead to the formation of other excited-state species or to decay through other low-lying conical intersection points. In Figures 9 and 10, we show the geometries of five optimized transition structures (TS_{CH_2}, $TS_{Z/E}$, $TS_{c/t}$, $TS_{CI_{c/t}}$, and $TS_{CI_{Z/E}}$) which define such alternative routes.

While the TS_{CH_2}, $TS_{Z/E}$, and $TS_{c/t}$ structures shown in Figure 9 define three simple isomerization processes which occur adiabatically on the $2A_1$ potential energy surface, the $TS_{CI_{c/t}}$ and $TS_{CI_{Z/E}}$ structures connect the *cZc*-HT* minimum to two different conical intersection points $CI_{c/t}$ and $CI_{Z/E}$. In Figure 10, we show the geometrical changes occurring along the IRC corresponding to these last processes. These IRC's terminate immediately after $TS_{CI_{c/t}}$ and $TS_{CI_{Z/E}}$ at the $CI_{c/t}$ and $CI_{Z/E}$ conical intersections. The presence of a transition state along these paths implies that $CI_{c/t}$ and $CI_{Z/E}$ are both "peaked" conical intersections (see Scheme 3). There is little doubt that, while the analogue of the *cZc*-HT* → CI_{CHD} path cannot be found in the *tZc*-HT and *tZt*-HT conformers (i.e., the terminal carbons, C_1 and C_6 are too far away), a path to $CI_{c/t}$- and $CI_{Z/E}$-like conical intersections can be located for any possible conformer of hexatriene. We have recently reported a detailed investigation of this type of reaction path for the case of the photochemical isomerization of the conformer *tZt*-HT.[17] In this system the IRC and the $CI_{c/t}$ and $CI_{Z/E}$ structures are very close to those found for *cZc*-HT.

The CAS-SCF DZ+d energetics of the five pathways discussed above are illustrated in Figure 11. The computed energy barriers along these routes are found to be more than 1 order of magnitude higher than the barrier to CI_{CHD} (see also Table 1). Single-point CAS-SCF/MP2 DZ+d computations of the $TS_{CI_{c/t}}$ and $TS_{CI_{Z/E}}$ energies are also included in Table 1. These results demonstrate that, at this level of theory, the *cZc*-HT* → $TS_{CI_{c/t}}$ and *cZc*-HT* → $TS_{CI_{Z/E}}$ barriers are 23 and 29 kcal mol^{-1} higher than the barrier to CI_{CHD}. It is therefore apparent that evolution along these five pathways cannot compete with the *cZc*-HT* → CI_{CHD} decay process. Consequently, the outcome of a photochemical reaction producing *cZc*-HT* is predicted to originate exclusively from the *cZc*-HT* → CI_{CHD} decay and the only effective radiationless decay process must occur at CI_{CHD}.

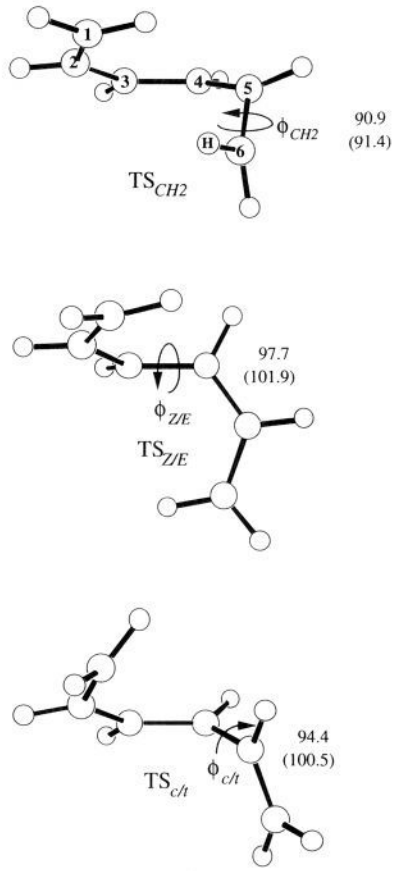

Figure 9. Optimized CAS-SCF equilibrium structures for the $2A_1$ adiabatic transition states TS_{CH_2}, $TS_{Z/E}$, and $TS_{c/t}$ connecting the *cZc*-HT* equilibrium structure to other excited-state conformational wells. The values of the relevant torsional parameters (ϕ_{CH_2} = C_4–C_5–C_6–H, $\phi_{Z/E}$ = C_2–C_3–C_4–C_5, and $\phi_{c/t}$ = C_3–C_4–C_5–C_6) are reported (in deg) for both the 4-31G and DZ+d (in brackets) results.

4. Comparison with Experimental Data

The "reference" mechanism for the rationalization of the CHD ring-opening (and HT ring-closure) experimental data was proposed by van der Lugt and Oosterhoff more than 30 years ago.[18] These authors concluded that, after photoexcitation, the reactant follows a relaxation route leading to an avoided-crossing minimum located halfway between the reactant and the product structures. The photoproduct is then generated by internal conversion of this excited-state intermediate to the ground-state surface. Computational investigations[14] along a reaction path interpolated between ground-state geometries have left this mechanistic picture completely unchanged. In contrast, our computational results indicate that the excited-state minimum which is populated after CHD* relaxation actually corresponds to $2A_1$ HT (i.e., *cZc*-HT*) and not to an avoided-crossing minimum. Further, the very efficient radiationless decay to the ground-state surface does not occur at this point but at the low-lying conical intersection CI_{CHD}. This decay point is therefore central to the mechanism of photochemical CHD ring opening.

It remains to compare our results with experimental data. We have divided this discussion into (i) a discussion of the CHD →

(17) Olivucci, M.; Bernardi, F.; Celani, P.; Ragazos, I.; Robb, M. A. *J. Am. Chem. Soc.* **1994**, *116*, 1077.

(18) Van der Lugt, W. T. A. M.; Oosterhoff, L. J. *J. Am. Chem. Soc.* **1969**, *91*, 6042–6049.

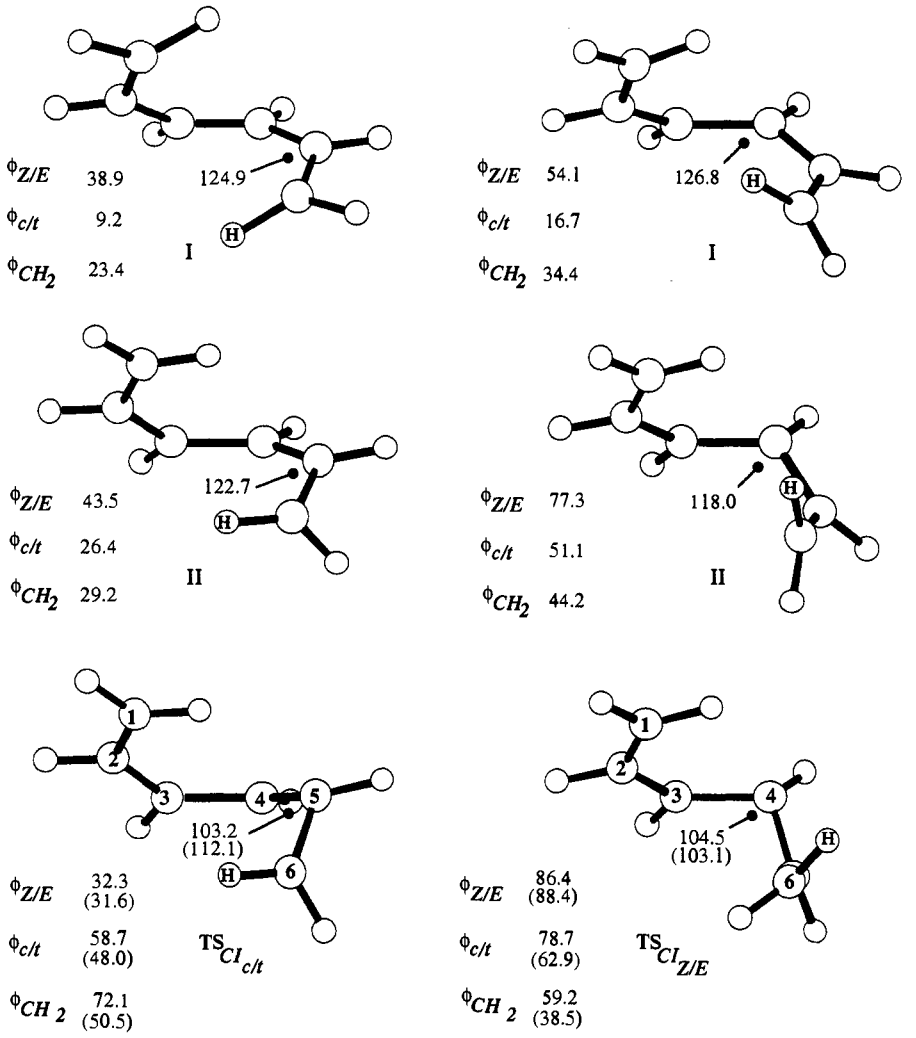

Figure 10. Evolution of the *cZc*-HT* equilibrium structure along two nonadiabatic IRC's computed at the CAS-SCF 4-31G level. Structures I and II are nonstationary point structures along the IRC connecting the reactant *cZc*-HT* to the two transition states $TS_{CI_{c/t}}$ and $TS_{CI_{Z/E}}$. The main structural parameters are reported (deg) for both the 4-31G and DZ+d (in brackets) results (ϕ_i torsions are defined in Figure 9). The DZ+d results are given for stationary points only.

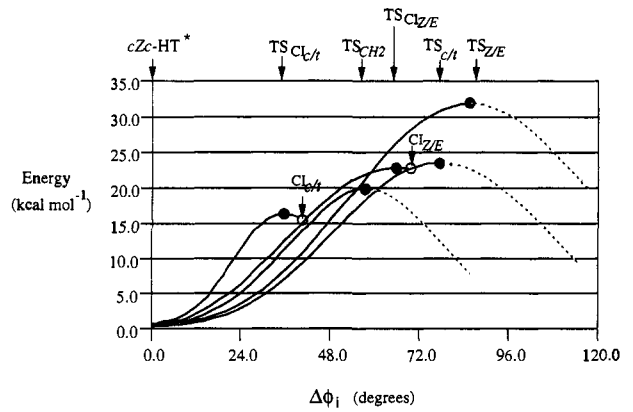

Figure 11. Comparison of the energy profiles of the five (three adiabatic and two nonadiabatic) *cZc*-HT* $2A_1$ isomerization pathways documented in this work. Black dots represent transition states (TS), and white dots represent conical intersection points (CI). Each energy profile is reported against the change ($\Delta\phi_i$) in the value of the associated torsional parameter (i = CH_2 for TS_{CH_2}, i = Z/E for $TS_{Z/E}$ and $TS_{CI_{Z/E}}$, and i = c/t for $TS_{c/t}$ and $TS_{CI_{c/t}}$).

cZc-HT quantum yield, (ii) a discussion of the origin of the picosecond *cZc*-HT appearance time, and (iii) a discussion of the CHD/HT photochemistry.

(i) Origin of the CHD → *cZc*-HT Quantum Yield. As remarked in section 3, the $2A_1$ and $1A_1$ energy profiles in Figure 6 demonstrate that CI_{CHD} has the local topology of a "sloped" conical intersection[9] where the excited-state IRC ultimately enters the branching space via a large-amplitude vibration along x_1 as shown in Figure 8. On the ground state, one has a sharp ridge along the same x_1 coordinate in the vicinity of CI_{CHD}. Since this ridge separates two different ground-state valleys, we expect a bifurcation of the reaction pathway to occur just after the $2A_1 \rightarrow 1A_1$ decay. This bifurcation rationalizes the quantum yield and the nature of the photoproducts observed, and we now proceed to elaborate on this point.

In classical terms,[11] a trajectory leaving the *cZc*-HT* involves motion along the IRC (i.e., toward CI_{CHD}) and a vibration in the orthogonal direction corresponding to the asymmetric stretching along x_2. At the conical intersection CI_{CHD}, the ground-state trajectory will continue in either the positive or negative direction of x_2 depending on the initial phase of the stretching vibration. This feature is indicated by the arrows in Figure 8. In fact, the asymmetric stretching of the carbon framework is the major effect responsible for the 2Ag/1Ag vibronic coupling observed in polyenes.[19]

The nature of the ground-state photoproducts originating from the pathway bifurcation illustrated in Figures 1 and 8 must be consistent with the nature of the geometrical change induced by motion in the x_2 direction (i.e., the asymmetric stretching of the

(19) (a) Zerbetto, F.; Zgierski, M. Z.; Negri, F.; Orlandi, G. *J. Chem. Phys.* **1988**, *89*, 3681. (b) Negri, F.; Orlandi, G.; Zerbetto, F.; Zgierski, M. Z. *J. Chem. Phys.* **1989**, *91*, 6215.

Scheme 4

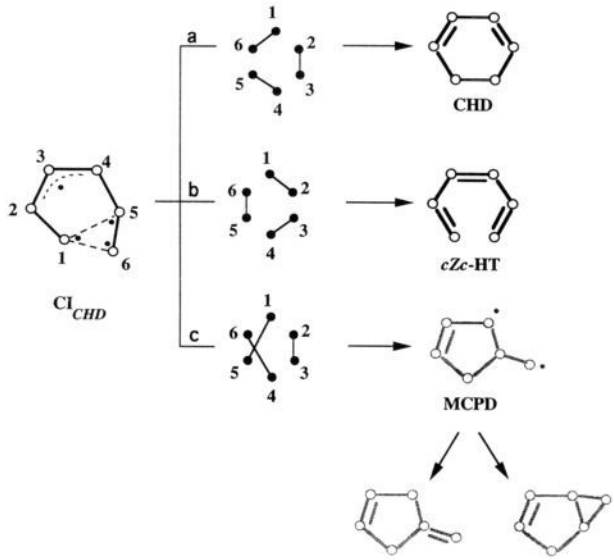

carbon framework). The first photoproduct is the result of a ground-state relaxation motion leading to formation of the C_1–C_2, C_3–C_4, and C_5–C_6 double bonds and ultimately resulting in the formation of *cZc*-HT. The second photoproduct is produced by relaxing the system in the opposite direction by forming the C_2–C_3 and C_4–C_5 double bonds and the C_1–C_6 single bond leading to back-formation of CHD. The observable consequence of this splitting is a reduction of the quantum yield of *cZc*-HT. The 0.406 *cZc*-HT quantum yield observed during CHD photolysis[2] is thus consistent with the structure of the CI_{CHD} branching space.

The driving force for the two different ground-state relaxation channels departing from CI_{CHD} is also consistent with its electronic structure. As the system begins to relax on the ground-state sheet, the associated wave function rapidly looses its tetraradical character as the four almost-unpaired electrons recouple. The electron recoupling and bond formation provide the driving force for ground-state relaxation. Thus the different ground-state channels departing from CI_{CHD} are located along coordinates which describe the evolution of the molecular structure of the system during electron recoupling. The possible electron recoupling processes of CI_{CHD} are illustrated in Scheme 4.

Route a describes a process which leads to CHD back-formation via coupling of the C_1, C_6 and C_4 (allyl), C_5 electrons. In contrast, route b describes a process leading to *cZc*-HT production via coupling of the C_1, C_2 (allyl) and C_5, C_6 electrons. These two processes are obviously associated with the two steepest descent directions shown in Figure 8. A third possible recoupling process may also take place via coupling of the C_1, C_5 electrons only, generating a ground-state methylcyclopentene diradical (MCPD) intermediate. This, presumably unstable diradical may then undergo ground-state reactivity, generating 3-methylenecyclopentene (via [1,2] H-shift) and/or bicyclohexane (via radical pairing). However, formation of MCPD is not predicted to be very effective. The shape of the lower sheet in Figure 8 suggests that initial motion toward MCPD would proceed along an initial uphill direction as it implies continuing on the ground state the motion along the excited-state IRC. Therefore, the detection of such photoproducts, possibly after long irradiation time, would provide evidence of the rather detailed mechanistic process proposed above. However, as far as we know, 3-methylenecyclopentene or bicyclohexane formation has never been observed during CHD photolysis. Our computations suggest that such products may be formed only if a large excess of vibrationally energy is concentrated along the *cZc*-HT* → CI_{CHD} mode, thus providing enough momentum along the corresponding IRC. Upon conventional photoexcitation, this seems unlikely as the initial CHD* → *cZc*-HT* relaxation will occur along a direction orthogonal to *cZc*-HT* → CI_{CHD} and therefore this channel becomes populated only by energy redistribution among the other vibrational mode of the system.

(ii) Origin of the Picosecond *cZc*-HT Appearance Time. The structure of CHD* (see Figure 2) demonstrates that this species is essentially a constrained excited-state butadiene. In fact, both the geometrical and electronic structures of the C_2–C_3–C_4–C_5 fragment are basically the same as those of the C_2 minimum found on the $2A_1$ excited-state surface of *s-cis*-butadiene.[7g,i] Further, the C_1–C_6 σ-bond in CHD* is only slightly stretched (1.6 Å). This suggests that the main locus of CHD photoexcitation is the butadiene moiety and that CHD* is the primary product of the $1B_2 \rightarrow 2A_1$ radiationless decay. The experimental results indicate decay to a C_2 structure with similar characteristics. The analysis of CHD resonance Raman spectra by Mathies et al.[1c] shows that, during $1B_2$ relaxation, there is a reduction of the C_2–C_3 and C_4–C_5 double-bond bond orders accompanied by torsional deformation. The data of Mathies et al. also indicate that at the moment of the decay the C_1–C_6 bond length is displaced only 0.05–0.1 Å from the original value and that the axial methylene C_1–H and C_6–H bonds are rotated 5–10°. Our results are consistent with these experimental findings. Comparison of the ground-state CHD-optimized geometrical parameters with those of the corresponding CHD* structure (see Figure 2a,b) shows a 0.13 Å double-bond length increase accompanied by a 17.0° increase of the double-bond torsion. Further the CHD → CHD* C_1–C_6 stretching and C_5–H and C_6–H wagging deformations are in the range indicated by the experiment.

After the CHD* has been generated via $1B_2 \rightarrow 2A_1$ radiationless decay, the system begins to propagate on the $2A_1$ surface. The direction of propagation is unambiguously established by the computational results reported in the previous section. CHD* propagates along the barrierless ring-opening IRC illustrated in Figure 4, ultimately leading to formation of *cZc*-HT*. According to spectroscopic data,[1] CHD* would enter the conrotatory ring-opening path with a substantial amount of kinetic energy due to the force applied in this direction by the $1B_2$ force field. Our computations suggest that this kinetic energy will further increase along the $2A_1$ path due to the exothermicity of the ring-opening process. Despite the fact that the system will accumulate an excess energy of >13 kcal mol^{-1} along the conrotatory ring-opening coordinate, the shape of the *cZc*-HT* well indicates that this motion will cause no further transformation of the system. The resulting vibrational excess energy will be rapidly redistributed among all degrees of freedom of the system or lost by interaction with the solvent molecules. Since fast internal conversion at the *cZc*-HT* equilibrium structure must be negligible due to the large (32 kcal mol^{-1}) $2A_1$–$1A_1$ energy gap,[20] the system is likely to equilibrate on a <1 ps time scale.

The qualitative discussion of the CHD* → *cZc*-HT* relaxation process given above leads to the conclusion that the $2A_1$ excited-state lifetime is determined by the rate of decay of *cZc*-HT*.

(20) Semiclassically, the probability of radiationless decay via the Landau–Zener model as shown by Desouter-Lecomte and Lorquet (Desouter-Lecomte, M.; Lorquet, J. C. *J. Chem. Phys.* **1979**, *71*, 4391, 3661) is given as

$$P = \exp[-(\pi/4)\xi]$$

where ξ is the Massey parameter given as

$$\xi = \frac{\Delta E(q)}{\frac{h}{2\pi}|\dot{\mathbf{q}}||g(\mathbf{q})|}$$

where q is a vector of nuclear displacement coordinates. The term $g(\mathbf{q})$ is the nonadiabatic coupling matrix element defined as

$$g(\mathbf{q}) = \langle \psi_1 | \partial \psi_2 | \partial \mathbf{q} \rangle$$

while $|\mathbf{q}|$ is the magnitude of the velocity along the reaction path $\mathbf{q}$ and ΔE is the energy gap. Unless ΔE is less than about 2 kcal mol^{-1}, the decay probability is vanishingly small. However, as we approach a point where the surfaces cross, the decay probability becomes unity.

According to our computations, the most efficient *cZc*-HT* ($2A_1 \rightarrow 1A_1$) decay route corresponds to the radiationless decay via the CI_{CHD} conical intersection. This conical intersection is easily accessed along the lowest-frequency normal mode of *cZc*-HT* as already discussed in the previous section. Thus, this decay does not occur at a pericyclic minimum as required by the van der Lugh–Oosteroff mechanism[17] but rather involves *cZc*-HT* large-amplitude distortion toward CI_{CHD}.

The computations of the order of magnitude of the decay rate and, in turn, of the *cZc*-HT appearance time provide an indirect test of our proposed mechanism. The measured 6 ps appearance time and 0.406 quantum yield of *cZc*-HT indicate a *cZc*-HT* lifetime (i.e., $1/K_{decay}$) of $\sim$ 2.5 ps. Decay to the ground state occurs by overcoming the small ($\sim$1 kcal mol^{-1}) barrier to CI_{CHD} (see Figure 6b). The decay process can be treated approximately as a one-step unimolecular reaction where the CI_{CHD} structure operates as a transition state (or activated complex) between the excited-state "reactant" *cZc*-HT* and the ground-state "product" *cZc*-HT. The decay rate constant K_{decay} is thus evaluated by assuming the validity of the following relationship:

$$K_{decay} = Ae^{-\Delta E_{decay}/RT}$$

where the pre-exponential factor is $A = (kT/h)e^{-\Delta S_{decay}/RT}$. Assuming ΔE_{decay} = 1.0 kcal mol^{-1} and $A = kT/h$ (i.e., $\Delta S_{decay} = 0$), then $1/K_{decay} \sim 1.0$ ps. However the magnitude of $1/K_{decay}$ is very sensitive to the value of both ΔE_{decay} and A. We can improve this estimate using the zero-point energy correction and the effect of ΔS_{decay} on the pre-exponential factor A. Frequency computations carried out at the CAS-SCF/4-31G level give a -4.0 cal mol^{-1} K^{-1} ΔS_{decay} contribution and a 1.0 kcal mol^{-1} zero-point energy correction. These quantities are not accurate since the 4-31G basis set overestimates surface curvatures. Using these quantities, we may compute an upper limit for $1/K_{decay}$ to be 36.0 ps. In conclusion we expect the following relationship to hold:

$$1 \text{ ps} < 1/K_{decay} < 36 \text{ ps}$$

While the observed lifetime falls in the computed range, one should expect that the approximate rate model used (i.e., transition-state theory) will fail in the vicinity of a conical intersection point due to nonadiabatic effects.[5] In other words, because of the reduced energy gap, effective $2A_1 \rightarrow 1A_1$ decay is expected to begin along the *cZc*-HT* $\rightarrow$ CI_{CHD} path before the conical intersection is actually reached. However, this effect can be seen as a reduction of the "effective" barrier to the conical intersection point. Consequently, in agreement with the experiment, we should expect the true value of $1/K_{decay}$ to be closer to the lower rather than to the upper limit of the indicated range.

(iii) CHD/HT Photochemistry. The computational data presented in section 3 support the conjecture that *cZc*-HT* is a common excited-state intermediate in both the CHD and the *cZc*-HT photolysis. Recently, Christensen, Yoshihara, Bell, and Petek[13a] have detected weak fluorescence from the $2A_1$ excited state of *tZt*-HT. This result indicates that the lowest excited state of *Z*-HT has $2A_1$ symmetry. Consequently, direct irradiation of *cZc*-HT is expected to lead to efficient formation of *cZc*-HT* via a relaxation path involving straightforward changes in the equilibrium bond lengths of the system. There are two remarkable issues which follow from this idea. Firstly, under conditions which allow the thermal equilibration of *cZc*-HT*, the outcome of the CHD and *cZc*-HT photolyses must be exactly the same. This means that, in the case of totally efficient $1B_2 \rightarrow 2A_1$ decay (i.e., $\Phi_{1B_2 \rightarrow 2A_1} = 1$), the sum of the quantum yields of *cZc*-HT formed via CHD photolysis ($\Phi_{CHD \rightarrow cZc\text{-}HT}$) and CHD formed via *cZc*-HT photolysis ($\Phi_{cZc\text{-}HT \rightarrow CHD}$) must approach unity (i.e., $\Phi_{CHD \rightarrow cZc\text{-}HT} + \Phi_{cZc\text{-}HT \rightarrow CHD} \sim 1.0$). Thus, since $\Phi_{CHDA \rightarrow cZc\text{-}HT}$ is 0.406,[2] $\Phi_{cZc\text{-}HT \rightarrow CHD}$ is expected to have values near 0.6. The second issue is that *cZc*-HT and CHD must be the only primary photoproducts of the photolyses of CHD and *cZc*-HT, respectively. In the previous section, we have demonstrated that the energy barriers along the alternative isomerization pathways of *cZc*-HT* are significantly higher than the barrier to CI_{CHD}. Thus *cZc*-HT* decay should proceed exclusively via the CI_{CHD} decay channel. The only alternative primary photoproduct to CHD and *cZc*-HT generated via the CI_{CHD} channel is the MCPD diradical shown in Scheme 4. However, as argued above, the MCPD quantum yield is expected to be very small.

Quantum yield measurements are available for photolysis of cyclohexadienes or hexatrienes.[2] We now discuss this experimental evidence in the light of the proposed mechanism. The quantum yield of CHD produced via photolysis of the *cZc*-HT conformer has, in our knowledge, never been experimentally determined. This quantity is obviously not easily accessible due to the fact that this conformer is only a very minor fraction of the *Z*-HT equilibrium mixture.[21] In fact, the *tZt*-HT conformer dominates the *Z*-HT conformational equilibrium in the ground state. As a consequence, the measured quantum yield data necessarily reflect the outcome of the simultaneous photolysis of a mixture of the three possible *Z*-HT conformers (i.e., *tZt*-HT, *tZc*-HT, and *cZc*-HT). Accordingly, the photolysis of unsubstituted *Z*-HT, where the *tZt* conformation dominates, produces CHD in an extremely low quantum yield.[2] Similarly, the photolysis of (*Z*)-2,5-dimethylhexatriene, where the *cZt*-HT conformation dominates, shows only a small production (Φ = 0.014) of 2,5-dimethylcyclohexadiene.[21,22] A dominant *tZc* conformation has also been assigned to previtamin D.[2,23] This is again consistent with the small quantum yields observed for the ring closure to ergosterol (0.015) and lumisterol (0.030). In all the systems mentioned above, the sum of the observed quantum yields for the ring-closure and the ring-opening photoreactions is much lower than unity. However, CHD quantum yield data have been reported in the literature for a few constrained and substituted *Z*-HT systems where the *cZc*-HT conformation is dominant. In this case, the observed quantum yield for the corresponding CHD photoproduct is high and very close to the expected value of $1.0 - \Phi_{CHD \rightarrow Z\text{-}HT}$. Brouwer, Cornelisse, and Jacobs[22] have investigated the case of the photolysis of (*Z*)-2,5-di-*tert*-butylcyclohexadiene, where the two bulky *tert*-butyl groups shift the equilibrium of the *Z*-HT mixture toward the *cZc*-HT conformation. As a consequence, the measured values of $\Phi_{CHD \rightarrow Z\text{-}HT}$ and $\Phi_{Z\text{-}HT \rightarrow CHD}$ are 0.54 and 0.46, respectively, as shown in part a of Scheme 5.

This is, in fact, the result expected in the limit of the photolysis of pure *cZc*-HT. An even more impressive set of experimental data comes from the photolysis of parent and substituted $\Delta^{1,3}$-hexalins (see b, c, and d in Scheme 5). Burgstahler, Givens, et al.[24] have determined the quantum yields for the ring opening of three differently substituted *trans*-$\Delta^{1,3}$-hexalins and ring closure of the three corresponding cyclodecatrienes. The quantum yields of the direct (ring-opening) and reverse (ring-closure) reactions are in all cases roughly complementary as reported in Scheme 5. This behavior is obviously related to the fact that the cyclodecatriene system forces the embedded hexatriene moiety in the *cZc*-HT conformation.

The prediction that CHD and *cZc*-HT are the only primary photoproducts formed via *cZc*-HT* decay is supported, indirectly, by the effect of bulky substituents on the quantum yield of irreversible (or long-term irradiation) and cis–trans isomerization

(21) Brouwer, A. M. Ph.D. Thesis, University of Leiden, Leiden, The Netherlands, 1987.

(22) (a) Brouwer, A. M.; Cornelisse, J.; Jacobs, H. J. C. *J. Photochem. Photobiol., A* **1988**, *42*, 117. (b) Brouwer, A. M.; Cornelisse, J.; Jacobs, H. J. C. *J. Photochem. Photobiol., A* **1988**, *42*, 313.

(23) (a) Gottfried, N.; Kaiser, W.; Braun, M.; Fuss, W.; Kompa, K. L. *Chem. Phys. Lett.* **1984**, *110*, 335. (b) Dauben, W. G.; Share, P. E.; Ollmann, R. R., Jr. *J. Am. Chem. Soc.* **1988**, *110*, 2548.

(24) Matuszewski, B.; Burgstahler, A. W.; Givens, R. S. *J. Am. Chem. Soc.* **1982**, *104*, 6875.

Scheme 5

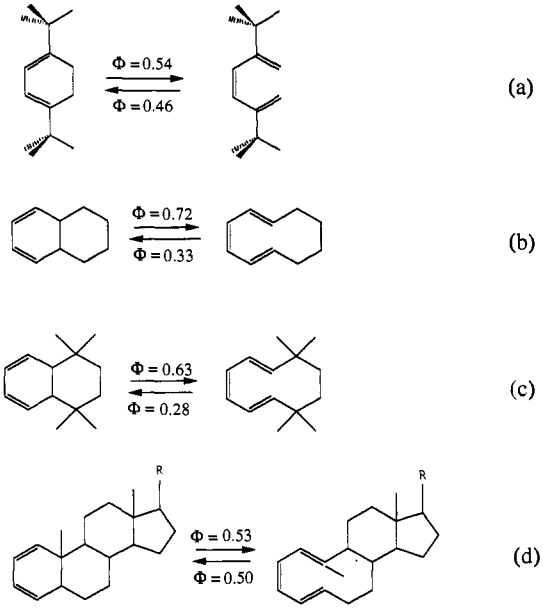

Scheme 6

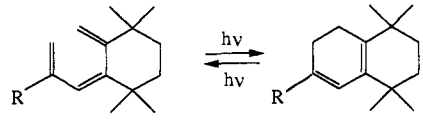

R = H, Me, *i*-Pr, *t*-Bu

photoproducts. Dauben et al.[25] have reported the quantum yields for the photolysis of a series of 3-substituted $\Delta^{3,5(10)}$-hexalins and corresponding trienes (see Scheme 6).

The results demonstrate that, when the substituent is –H, the most efficient process during the photolysis of the triene (direct reaction in Scheme 6) is the formation of the vinylbutadiene and bicyclo[3.1.0] derivatives. Only a very minor process leads to formation of the "CHD" ring-closure product $\Delta^{3,5(10)}$-hexalin. However, when a bulky substituent such –isopropyl is replaced by –H, then the major reaction becomes the formation of 3-isopropyl-$\Delta^{3,5(10)}$-hexalin. This effect is again rationalized on the basis of the change in the dominant conformation of the hexatriene moiety. This would shift the equilibrium from *tZc* to *cZc* when the substituent is –isopropyl. Remarkably, the reverse photoreaction (i.e., the photolysis of $\Delta^{3,5(10)}$-hexalins) shows a similar behavior. In fact, photolyses of $\Delta^{3,5(10)}$-hexalin and 3-methyl-, 3-isopropyl- and 3-*tert*-butyl-$\Delta^{3,5(10)}$-hexalin show decreasing rates of formation of the irreversible vinylbutadiene and bicyclo[3.1.0] derivatives as the size of the substituents is increased. These observations all support the idea that the irreversible photoproducts are formed via photolysis of *tZc* or *tZt* excited-state trienes and not directly via decay from the *cZc* excited-state well. In the case of the photolysis of $\Delta^{3,5(10)}$-hexalins, *tZc*-trienes would be only formed via fast ground-state cis–trans conformational isomerization of the *cZc* primary product as described by Mathies (see Scheme 1). Other quantum yield measurements support the same point of view. For instance, the quantum yields of 3-vinylcyclobutene and *E*-HT photoproducts dramatically decrease when the size of the 2,5-substituents in hexatrienes is increased.[24] In fact, photolyses of 2,5-dimethyl and 2,5-di-*tert*-butylhexatriene yield vinylcyclobutenes and *E*-hexatrienes with quantum yields of 0.04, 0.37 and 0.004, 0.052, respectively.

(25) Dauben, W. G.; Rabinowitz, J.; Vietmeyer, N. D.; Wendschuh, P. H. *J. Am. Chem. Soc.* **1972**, *94*, 4285.

5. Conclusions

Our computations demonstrate that the $2A_1 \rightarrow 1A_1$ decay channel of the van der Lugt–Oosterhoff[14,18] mechanism does not actually correspond to a $2A_1$ avoided crossing minimum (the so-called "pericyclic minimum"). In fact, decay from the $2A_1$ excited state to the ground ($1A_1$) state occurs at a conical intersection point CI_{CHD} after the CHD CH_2–CH_2 σ-bond has been completely broken. The rapid 10 fs depopulation of the spectroscopic ($1B_2$) state has been tentatively explained by Trulson[1b,c] by the existence of a $1B_2/2A_1$ conical intersection. Thus the photochemical ring opening of CHD would involve decay through two conical intersections which are entered sequentially during the reaction. After the $1B_2 \rightarrow 2A_1$ decay, the system relaxes toward the *cZc*-HT* $2A_1$ intermediate and then undergoes a second decay through CI_{CHD}.

The proposed mechanism is fully consistent with experimental data. The observed picosecond lifetime of CHD is consistent with the 1 kcal mol^{-1} decay barrier found at the CAS-SCF/MP2 level of theory (the $1B_2 \rightarrow 2A_1$ decay barrier must be negligible). The limited quantum yield observed for the production of ground-state *cZc*-HT is consistent with the shape of the ground- and excited-state energy sheets computed in the region of the CI_{CHD} point. According to our results, the system must undergo an efficient pathway branching either to the final product or back to the initial reactant immediately following the $2A_1 \rightarrow 1A_1$ decay.

The results of extensive computational investigations of the $2A_1$ potential energy surface indicate that *cZc*-HT must be the only primary photoproduct of the direct irradiation of CHD. Further, the *cZc*-HT* excited-state minimum must be a common intermediate in the CHD and *cZc*-HT photolyses. Therefore, in case of a near equilibration at the *cZc*-HT* excited-state well, photoproduct distribution from either species must be the same. This fact is consistent with experimental observations which show that when the *cZc* conformer dominates the ground-state conformational mixture of a *Z*-hexatriene the relationship $\Phi_{CHD \rightarrow Z\text{-}HT} \sim (1 - \Phi_{Z\text{-}HT \rightarrow CHD})$ holds.

Acknowledgment. This research has been supported in part by the SERC (U.K.) under Grant Number GR/J 25123. The authors are also grateful to IBM for support under a Joint Study Agreement. All computations were run on an IBM RS/6000.